Hydroxychloroquine: mechanism of action inhibiting SARS-CoV2 entry.

Zixuan Yuan[1,2,3,^], Mahmud Arif Pavel[1,2,^], Hao Wang[1,2,3], Scott B. Hansen[1,2,*]

[1]Department of Molecular Medicine, [2]Department of Neuroscience, [3]Skaggs Graduate School of Chemical and Biological Sciences, The Scripps Research Institute, Jupiter, Florida, 33458, USA

^ These authors contributed equally.
*Correspondence: Scott Hansen (Associate Professor, Molecular Medicine, The Scripps Research Institute 130 Scripps Way #C236 Jupiter, FL 33458, shansen@scripps.edu)

Abbreviated Title: Lipid raft mechanism of hydroxychloroquine.

Word and Element Counts: words (Abstract), words (Introduction), words (Discussion), 5 figures

ABSTRACT

Background: SARS-coronavirus 2 (SARS-CoV-2) is currently causing a worldwide pandemic. Potential drugs identified for the treatment of SARS-CoV-2 infection include chloroquine (CQ), its derivative hydroxychloroquine (HCQ), and the anesthetic propofol. Their mechanism of action in SARS-CoV-2 infection is poorly understood. Recently, anesthetics, both general and local, were shown to disrupt ordered lipid domains. These same lipid domains recruit the SARS-CoV-2 surface receptor angiotensin converting enzyme 2 (ACE2) to an endocytic entry point and their disruption by cholesterol depletion decreases ACE2 recruitment and viral entry.

Methods: Viral entry was determined using a SARS-CoV-2 pseudovirus (SARS2-PV) and a luciferase reporter gene expressed by the virus after treatment of the cells with 50 μM propofol, tetracaine, HCQ, and erythromycin. HCQ disruption of monosialotetrahexosylganglioside1 (GM1) lipid rafts, phosphatidylinositol 4,5-bisphosphate (PIP_2) domains, and ACE2 receptor at nanoscale distances was monitored by direct stochastic reconstruction microscopy (dSTORM). Cells were fixed, permeabilized, and then labeled with either fluorescent cholera toxin B (CTxB) or antibody and then fixed again prior to imaging. Cluster analysis of dSTORM images was used to determine size and number and cross pair correlation was used to determine trafficking of endogenously expressed ACE2 in and out of lipid domains.

Results: Propofol, tetracaine, and HCQ inhibit SARS2-PV viral entry. HCQ directly perturbs both GM1 lipid rafts and PIP_2 domains. GM1 rafts increased in size and number similar to anesthetic disruption of lipid rafts; PIP_2 domains decreased in size and number. HCQ blocked both GM1 and PIP_2 domains ability to attract and cluster ACE2.

Conclusions: We conclude HCQ is an anesthetic-like compound that disrupts GM1 lipid rafts similar to propofol and other local or general anesthetics. Furthermore, we conclude disruption of GM1 raft function, and not the concentration of GM1 raft molecules, governs the antiviral properties of HCQ. HCQ disruption of the membrane appears to also disrupt the production of host defense peptide, hence an antimicrobial such as erythromycin could be an important combined treatment. Nonetheless erythromycin has anti-SARS-CoV-2 activity and may combine with HCQ to reduce infection.

KEY POINTS

Question: What is the molecular basis for antiviral activity of hydroxychloroquine and propofol?

Findings: Hydroxychloroquine disrupt lipid rafts similar to local and general anesthetics.

Meaning: Since lipids cluster ACE2 and facilitate viral entry, hydroxychloroquine and anesthetics appear to inhibit viral entry by disrupting the lipid clustering and ACE2 localization.

INTRODUCTION

Coronavirus disease 2019 (COVID19), a viral infection caused by severe acute respiratory syndrome coronavirus 2 (SARS-CoV-2), recently emerged as a serious public health problem[1]. Currently, millions of people have been infected with SARS-CoV-2 worldwide. Treatments for severe symptoms include a well-known FDA approved antimalarial agents chloroquine (CQ) and its derivative hydroxychloroquine (HCQ) [2–6], but their molecular mechanism of action are poorly understood, their use is not without controversy[7]. In the treatment of malaria, CQ targets the replication cycle of the parasite[8], a mechanism of action presumably unrelated to their action in COVID19. The anesthetic propofol also has beneficial effects on COVID19 treatment and the FDA recently permitted the emergency use of Fresenius Propoven 2% emulsion to maintain sedation via continuous infusion for COVID-19 patients[9]. Understanding the underlying mechanism for these compounds in COVID19 could help in bettering implementation and designing efficacious clinical trials for establishing effective treatments.

We have shown a cholesterol-dependent mechanism for anesthetics that regulates the movement of membrane proteins between monosialotetrahexosylganglioside1 (GM1) containing lipid rafts and PIP_2 lipid domains[10,11]. The GM1 rafts are formed by cholesterol packing[12] and the PIP_2 domains are formed from charged protein clustering[13] (Fig. S1A). In cellular membranes, local and general anesthetics, including propofol, disrupt GM1 rafts[10,14].

Cholesterol is critical to both viral entry and an immune response[15]. We recently showed the SARS-CoV-2 surface receptor, angiotensinogen converting enzyme 2 (ACE2)[16,17] moves between GM1 rafts and PIP_2 domains in a cholesterol dependent manner[18]. In an obese mouse model, cholesterol was high in lung tissue and this correlated with ACE2 translocation to endocytic lipids, a condition that accelerated viral entry into the target cells in cell culture[18].

Interestingly, CQ is an anesthetic—subcutaneous injection of CQ produces instant local anesthesia sufficient to perform a surgical procedure[19,20] and structurally CQ is strikingly similar to a local anesthetic (Fig. 1A). Both CQ and local anesthetics such as tetracaine are weak bases and their uptake changes the acid base balance within the membrane[21,22]. Additionally, common local anesthetics such as mepivacaine, bupivacaine, tetracaine and other lipid raft disrupting compounds, such as sterols and cyclodextrin, can exert anti-viral or anti-microbial activity[23–26].

These properties led us to compare the drugs' lipid disruption properties with viral entry and potentially understand at least a component of their underlying molecular mechanism. Understanding CQ's mechanism of action could help understanding potential contradictions and determining which cellular and animal models are appropriate for testing CQ's effect *in vitro* and *in vivo*. Here we employed super resolution imaging to show that HCQ disrupts GM1 rafts in a manner similar to anesthetics causing ACE2 to leave GM1 rafts (the endocytic site of viral entry) and PIP_2 domains.

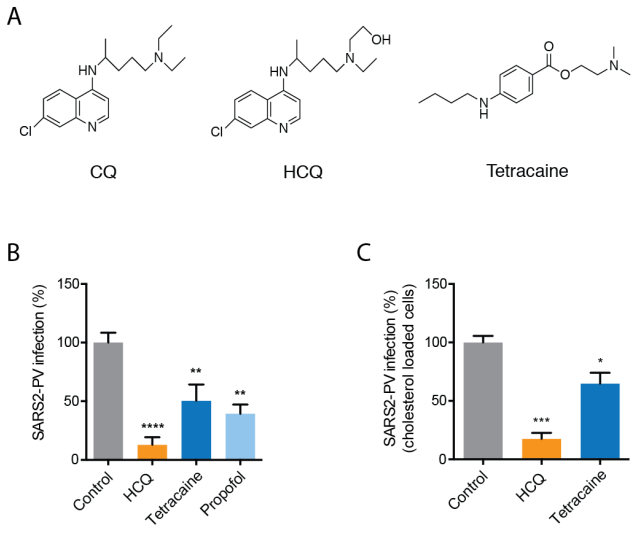

Fig. 1. Anesthetics and hydroxychloroquine inhibit SARS2-PV entry. (A) Chemical structures comparing chloroquine (CQ) and hydroxychloroquine (HCQ) to tetracaine, a local anesthetic. **(B-C)** SARS-CoV-2 pseudovirus (SARS2-PV) entry assay measured as a percent of control luciferase activity. HCQ (50 μM), tetracaine (50 μM) and propofol (50 μM) inhibited viral infection in HEK293T cells withiout (B) and with (C) cholesterol loading (4 μM apolipoprotein E + 10% serum). Data are expressed as mean ± s.e.m., *P ≤ 0.05, **P ≤ 0.01, ***P ≤ 0.001, ****P ≤ 0.0001, one-way ANOVA, n=3-5.

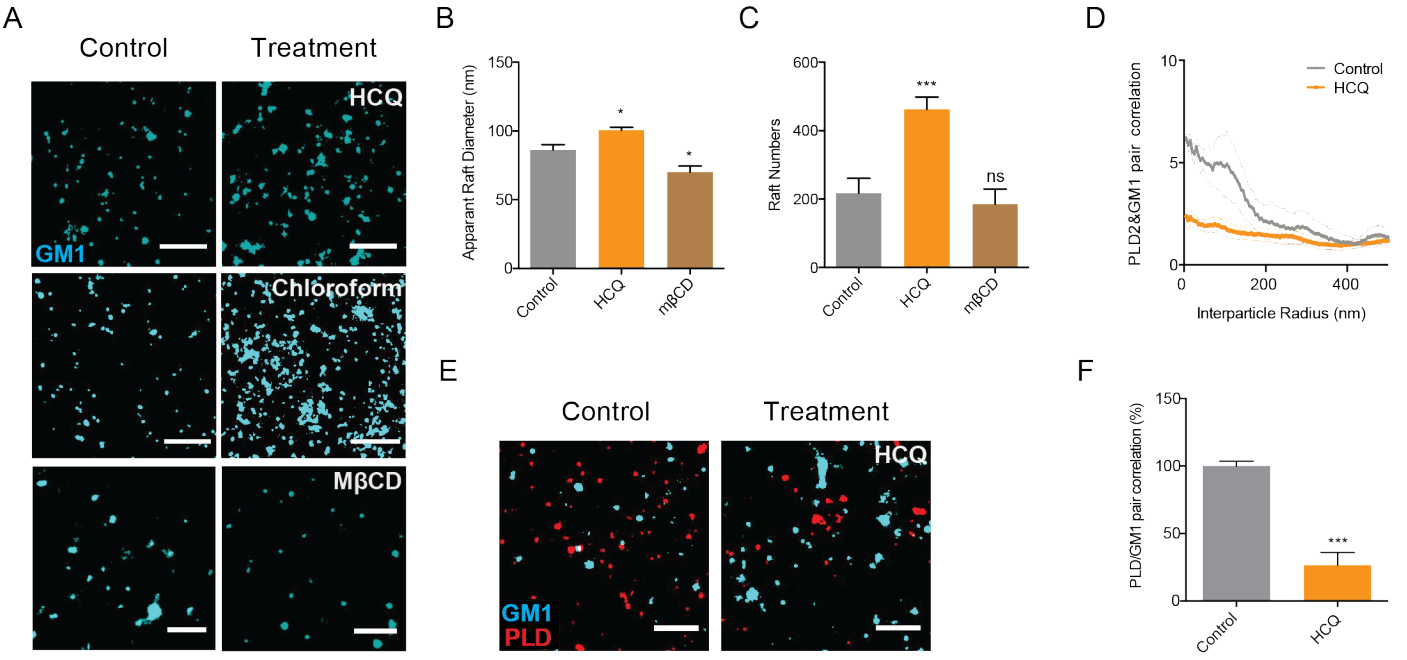

Fig. 2. Hydroxychloroquine disrupts GM1 rafts. (A) Representative dSTORM images showing the GM1 raft perturbation by HCQ (50 μM) and MβCD (100 μM) in HEK293T cells (Scale bars = 1 μm). Similar disruption from 1 mM chloroform treatment, an anesthetic, is shown from Pavel et. al. PNAS 2020; 117:13757–66, with permission, for comparison. **(B-C)** Bar graph of the apparent raft diameter analyzed by DBSCAN cluster analysis. HCQ increases both raft diameter (B) and number (C) of GM1 rafts. Data are expressed as mean ± s.e.m., *P ≤ 0.05, ***P ≤ 0.001, one-way ANOVA, n=7. **(D-E)** Cross pair correlation analysis (D) of two color dSTORM imaging (E). HCQ treatment decreased association of phospholipase D2 (PLD2, red shading), an anesthetic sensitive enzyme, with GM1 rafts (cyan shading) (scale bars = 1 μm). **(F)** Quantification of cross pair correlation in (D) at short distances (0-5 nm). Data are expressed as mean ± s.e.m., ***P ≤ 0.001, unpaired t-test, n=4-7.

RESULTS

Inhibition of SARS-CoV2 entry by anesthetic-like compounds.

In order to test SARS-CoV2 viral entry, we expressed a retrovirus pseudotyped with the SARS2 spike protein (SARS2-PV) in HEK 293T cells. A segment of the spike protein binds to ACE2 and recapitulates viral entry[27,28]. A luciferase encoded in the pseudotyped virus allows quantitative measurement of viral entry.

Treatments with propofol, tetracaine, and HCQ all robustly reduced SARS2-PV entry into HEK293T cells overexpressing ACE2 receptor (Fig. 1B). The cells were first treated with drug (50 μM) and then the drug was removed, after which SARS2-PV was applied (*i.e.*, the virus did not experience the drug directly, only the cells). HCQ had the greatest effect with almost a 90% reduction in SARS2-PV luciferase activity (Fig. 1B).

Since COVID19 is often severe in obese patients, we also tested HCQ inhibition in cells loaded with cholesterol. To load cells with cholesterol, we treated HEK293T cells with 4 μM apolipoprotein E (ApoE) and 10% serum. ApoE is a cholesterol carrier protein linked to Alzheimer's and the severity of COVID19[29]. In tissue, ApoE binds to low-density lipoprotein (LDL) receptor and facilitates loading of cholesterol into cells[30] (Fig. S1B). Both HCQ and tetracaine reduced SARS2-PV in high cholesterol conditions. Cholesterol slightly reduced their potency, but the effect was not statistically significant (Fig. 1C).

HCQ acts in the anesthetic pathway.

Based on the structural similarities of HCQ with anesthetics (Fig. 1A), we investigated HCQ's ability to function as an anesthetic. We recently showed a mechanism of anesthesia based on disruption of lipid rafts. Anesthetics perturb rafts in two ways. First, anesthetics increase the apparent size and number of lipid rafts as observed using super resolution imaging and cluster analysis[10,14].

Second, anesthetics can disassociate cholesterol sensitive proteins from GM1 rafts. The disassociation of a proteins from a GM1 raft can also be measured with super resolution imaging using cross pair correlation analysis. The results of cross pair correlation are quantitative, well established, and provide mechanistic insights into protein localization and raft associated signaling[10,14].

To test HCQ's effects on lipid membranes, we first examined the effect of HCQ on the apparent structure (size and number) of GM1 rafts by direct stochastic optical reconstruction microscopy (dSTORM) in the membranes of HEK293T cells using density-based spatial clustering of applications with noise (DBSCAN). We found 50 μM HCQ, a physiologically relevant concentration that inhibits viral infection, increased the number and apparent size (Fig. 2A-C) of GM1 rafts. HCQ's perturbation was very similar to that previously seen for general anesthetics chloroform and isofluorane[10] (Fig. 2A). We also observed Ripley's H(r) of GM1 clusters decreased after HCQ treatment (Fig. S2A), suggesting a decrease in domain separation. Methyl-beta cyclodextrin (MβCD), a chemical known to deplete GM1 rafts from the cell membrane, decreased both the number and apparent size of GM1 clusters (Fig. 2A-B).

To test HCQ for anesthetic-like properties, we treated HEK293T cells with 50 μM HCQ, labeled GM1 lipids and the protein phospholipase D2 (PLD2) with (CTxB, a pentadentate toxin that labels GM1 lipids and anti PLD2 antibody respectively). Phospholipase D2 (PLD2) is an anesthetic sensitive enzyme that translocates out of GM1 rafts in response to general anesthetics xenon, chloroform, isoflurane, propofol, and diethyl ether. Furthermore, mutant flies lacking PLD2 are resistant to anesthesia[10,31] and thus provides a test for anesthetic like effects in the membrane.

We found 50 μM HCQ robustly disrupted PLD2 localization with GM1 rafts (Fig. 2D-E). Quantification of the % cross pair correlation at short radiuses (0-5 nm) decreased by almost 70% (Fig. 2F). In a live cell PLD2 assay, HCQ inhibited enzymatic activity (Fig. S2B-C) a result similar to local anesthetic tetracaine, but opposite the effect of general anesthetics[14]. Hence HCQ's effect on the lipid membrane is similar to general anesthetics (Fig. 2A) while its effect on PLD2 is similar to local anesthetics[14].

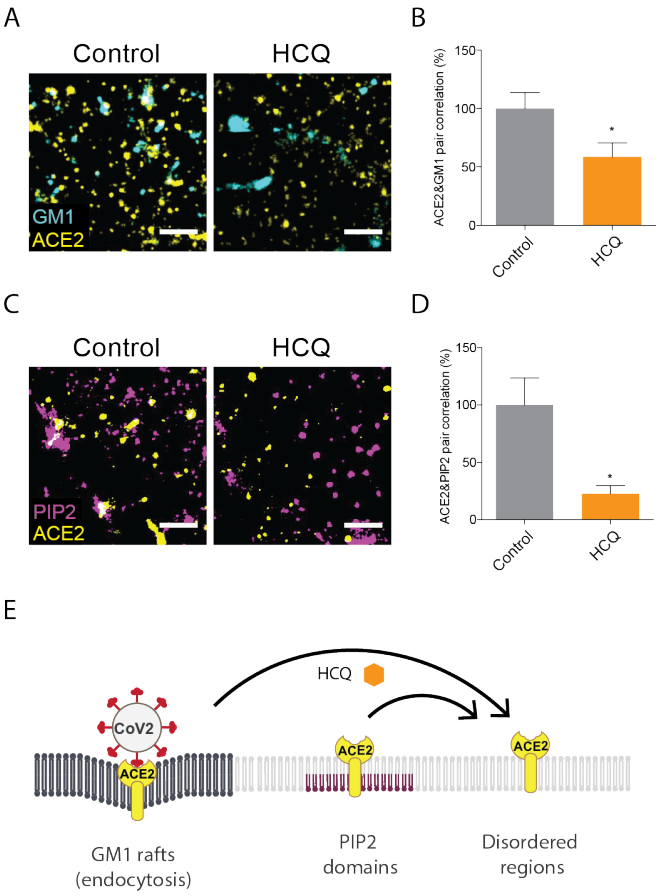

Fig. 3. Hydroxychloroquine moves ACE2 from GM1 rafts and PIP_2 domains. (A) Representative dSTORM super resolution images showing the effect of HCQ (50 μM) on the nanoscale localization of ACE2 (yellow) with GM1 rafts (cyan) after loading HEK293T cells with cholesterol (scale bars = 1 μm). **(B)** Percent of cross pair correlation (Fig. S3A) calculated at short distances (0-5 nm). HCQ decreased the cross pair correlation between ACE2 and GM1 rafts indicating a decrease in association between PLD and GM1 rafts. Data are expressed as mean ± s.e.m., *P ≤ 0.05, unpaired t-test, n=6. **(C)** Representative dSTORM super resolution images of ACE2 (yellow) and PIP_2 domain (magenta) in HEK293T cells at normal cholesterol level after the treatment of HCQ (50 μM) (scale bars = 1 μm). **(D)** HCQ decreased the cross pair correlation between ACE2 and PIP_2 domains indicating a decrease in association between PLD and PIP_2 domains. Data are expressed as mean ± s.e.m., *P ≤ 0.05, unpaired t-test, n=5. **(E)** Model showing HCQ (orange hexagon) inducing translocation of ACE2 (yellow receptor) from GM1 rafts (dark grey lipids) in high cholesterol. HCQ disrupts ACE2 interaction with PIP_2 domains causing ACE2 to translocate to the disordered region.

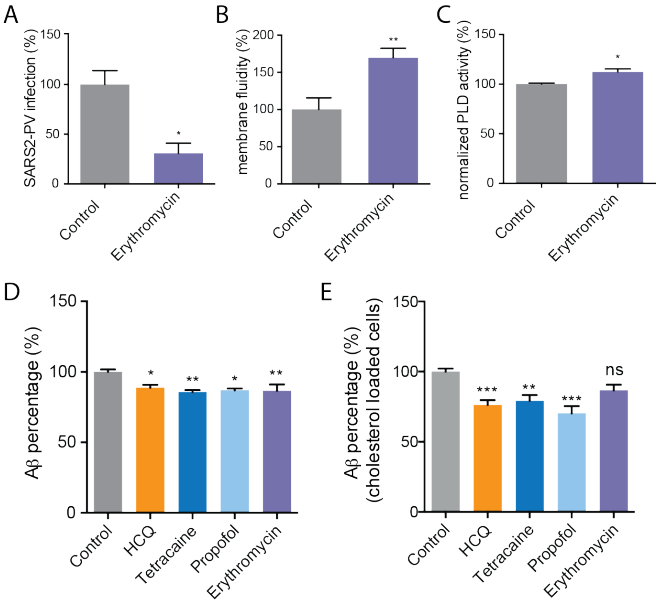

Fig. 4. Erythromycin inhibits SARS-CoV-2 viral entry. (A) Percent SARS-CoV-2 pseudovirus (SARS2-PV) infection after erythromycin (100mg/ml) treatment of HEK293T cells over expressing ACE2. Data are expressed as mean ± s.e.m., *P ≤ 0.05, unpaired t test, n=3. **(B)** Erythromycin (100mg/ml) increased membrane fluidity in membrane fluidity assay. Data are expressed as mean ± s.e.m., **P ≤ 0.01, unpaired t test, n=3-4. **(C)** A raft disruption assay based on PLD2 enzymatic activity in HEK293T cells. **(D-E)** An ELISA assay showing HCQ (50 μM), tetracaine (50 μM), propofol (100 μM), and erythromycin (100μg/ml) decreased the synthesis of Ab40 in HEK293T cells with (E) and without (D) cholesterol loading (4 μM apolipoprotein E + 10% serum). Data are expressed as mean ± s.e.m., *P ≤ 0.05, **P ≤ 0.01, one-way ANOVA, n=3-7.

HCQ disrupts clustering of ACE2 with GM1 rafts.

Next we asked if the anesthetic effects of HCQ on lipid membranes contribute to its antiviral properties. To recapitulate an *in vivo* environment of obese patients, we loaded HEK293T cells with cholesterol using apoE and serum[18], fixed the cells, labeled them with anti-ACE2 antibody and CTxB, and imaged using dSTORM.

After 50 μM HCQ treatment, we found ACE2 receptor dramatically decreased its association with GM1 rafts, despite the increase in GM1 raft size and number (Fig 3A). Cross pair correlation was decreased at all distances (Fig. S3A). At short distances (0-5 nm) the decreased was almost 50% ($p<0.05$) (Fig. 3B) suggesting HCQ disrupts the ability of GM1 rafts to sequester ACE2.

HCQ disrupts PIP_2 domains

We have previously shown that disrupting GM1 rafts moves ACE2 to and clusters with PIP_2 domains[18]. We presume PIP_2 domains reside in the disordered regions away from GM1 rafts due to the large number of unsaturations in its acyl chains[32,33]. To determine whether ACE2 clusters with PIP_2 domains after HCQ disrupts GM1 rafts, we co-labeled ACE2 and PIP_2 domains in HEK293T cells at normal cholesterol levels and treated the cells with and without 50 μM HCQ. Figure 2D shows representative figures of dSTORM imaging. Somewhat unexpected, the cross pair correlation between ACE2 and PIP_2 domains clearly decreased with HCQ treatment (Fig. 2E), suggesting HCQ disrupts ACE2 association with both GM1 rafts and PIP_2 domains.

We further characterized the nature of the PIP_2 disruption by analyzing the structures of the PIP_2 domains before and after HCQ treatment using dSTORM cluster analysis. Figure 2D shows representative dSTORM images comparing PIP_2 domains before and after HCQ treatment. HCQ treatment decreased both the number and size of PIP_2 domains confirming HCQ directly perturbs the domains (Fig. S3B-C).

Erythromycin inhibits viral entry through perturbing GM1 rafts

Azithromycin, an antibiotic derived from erythromycin, has been given to COVID-19 patients in combination with HCQ and was shown to significantly reduce COVID-19 associated mortality[34]. We tested SARS2-PV infection in HEK293T cells over expressing ACE2 and found the antibiotic alone decreases viral entry (Fig. 3A). To test for a perturbation to lipids, we measured membrane fluidity and activation of PLD2. Erythromycin increased both membrane fluidity (Fig. 4B) and PLD2 activity (Fig. 4C), consistent with raft disruption. However, when we examined the cross pair correlation of ACE2 and GM1 correlation after erythromycin treatment in high cholesterol we saw increased association of ACE2 with GM1 (Fig. S3D-E), which is opposite expected for raft disruption and may suggest an alternative or more complicated effect in high cholesterol.

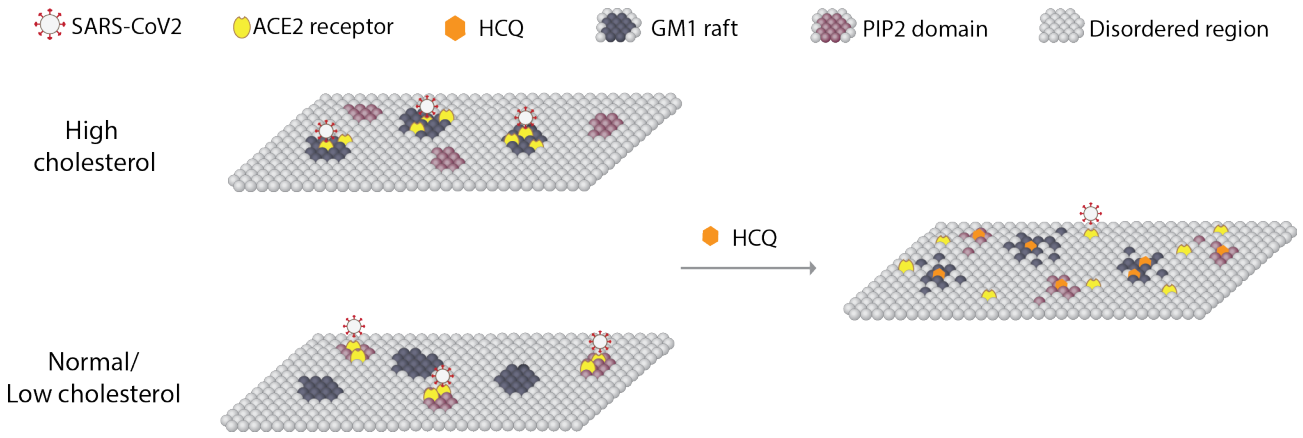

Fig. 5. Model for HCQ mechanism of action in SARS-CoV-2 infectivity. A representation of the plasma membrane shows nanoscale lipid heterogeneity. Saturated monosialotetrahexosylganglioside1 (GM1) lipid rafts (dark grey) attract ACE2 (yellow oval) in high cholesterol (top). In low or normal cholesterol, ACE2 associates primarily with phosphatidylinositol 4,5-bisphosphate (PIP_2). Hydroxychloroquine (HCQ, orange hexagon) disrupts the lipid order and excludes the association of ACE2 from both GM1 rafts and PIP_2 domains (right panel). The SARS-CoV-2 virus (white circle with red spike) binds to the ACE2 receptor. The location of the ACE2 receptor dictates the location and efficacy of viral entry.

HCQ's disruption on host defense peptides.

Lastly, we considered HCQ effect on host defense peptides. Host defense peptides are amphipathic antimicrobial peptides that are upregulated during an immune response and perturb the membranes of microbes[35,36]. Cholesterol and raft integrity are of great importance to the modulation of both innate and acquired immune responses[37]. Amyloid-beta (Aβ) has been demonstrated to protect against microbial infection as a host defense peptide and the production of Aβ is regulated by lipid raft integrity[38,39] (Fig. S1C). We hypothesized that if HCQ disrupts lipids, it may also disrupt the production of host defense peptides, thereby necessitating an antibiotic to mitigate this deleterious side effect.

To investigate the role of HCQ and anesthetics-induced raft perturbation in the synthesis of host defense peptides, we measured Aβ production using a sandwich enzyme-linked immunosorbent assay (ELISA). We found that HCQ reduced Aβ generation ~ 10% in cultured HEK293T cells (Fig. 4D). The effect was statistically significant ($p<0.05$). We then loaded HEK293T cells with cholesterol (apoE + serum) to better reflect the disease state of COVID-19 with severe symptoms. The reduction of Aβ was ~20% greater in high cholesterol. Since tetracaine and propofol also disrupt GM1 rafts, we tested their effect on Aβ production and found it to be very similar in both high and low cholesterol. Interestingly, erythromycin did disrupt Aβ production in low cholesterol, but in high cholesterol the effect was very small and not statistically significant.

DISCUSSION

Taken together our finding shows a component of HCQ acts through anesthetic-like mechanism that disrupts ACE2 localization at both GM1 rafts and PIP_2 domains. The decrease in Aβ suggests a rationale for administrating an antibiotic in combination with HCQ in patients with COVID19. Our findings also suggest that HCQ may be able to reverse some of the adverse effects of high cholesterol loading common to high-risk patients. These results suggest that clinical studies with HCQ should look for benefits in high-risk patients (i.e., patients with high tissue cholesterol). Animal and cultured cell experiments in low cholesterol likely fail to capture the full benefit of HCQ and should be carefully scrutinized.

Based on the imaging data showing ACE2 moving out of GM1 rafts and PIP_2 domains, we propose a model of HCQ disrupting SARS-CoV-2 viral entry through raft perturbation (Fig. 5). In an inflamed state, cholesterol traffics ACE2 from PIP_2 domains to GM1 rafts where virions dock and enter through endocytic pathway. The perturbation of both GM1 rafts and PIP_2 domains by HCQ likely inhibits viral entry by making it more difficult to cluster ACE2 and enter the endocytic entry point. The mechanism of surface receptor

clustering was recently shown to be important to the related influenza virus[40].

Testing ACE2 association with GM1 rafts in the presence of HCQ should distinguish the direct role of cholesterol concentration from GM1 function. Since the area of GM1 rafts increased, the exit of ACE2 from the GM1 raft and PIP_2 domains appears to be the key mechanism, and not the increase of GM1 raft lipids (cholesterol and sphingomyelin).

The tertiary amine likely imbues HCQ with its local anesthetic-like properties and the positively charged amine likely interacts directly with PIP_2 to block ACE2 localization with PIP_2. It is unclear where ACE2 resides when it is excluded from both GM1 rafts and PIP_2 domains. Presumably it moves into a generic disordered region of the cell membrane. Alternatively, it may move into PIP_3 domains. PIP_3 is typically short chain saturated[32,33] and could possibly attract ACE2 if HCQ preferentially disrupts long chain polyunsaturated lipids such as PIP_2.

Erythromycin, an analog of azithromycin, also contains a tertiary amine. Other aminoglycosides (e.g. neomycin) are known to bind tightly to and scavenge PIP_2. Scavenging PIP_2 is normally thought to block ligand binding[41] or change a surface charge. Our data here suggests hydrophobic charged molecules disrupt PIP_2 and the resulting ACE2 clustering. We previously assumed the inhibition of PLD2 by tetracaine was through direct binding of tetracaine to the enzyme, but here HCQ did not inhibit purified cabbage PLD (Fig. S2D), suggesting the inhibition could also occur through disruption of PIP_2 and its ability to bind PLD2.

The results of HCQ and anesthetics reducing the production of Aβ, a host defense peptide, provide a rational to supply exogenous antibiotics in combination with HCQ so that the overall antibiotics level is maintained. This is consistent with clinical observations that azithromycin reinforces the effect of HCQ[34].

A previous mechanism suggested that HCQ could inhibit SARS-COV-2 viral entry step by changing the glycosylation of membrane proteins[42,43]. Our raft-associated protein activation mechanism is consistent with changes in glycosylation if the glycosylated protein is also sensitive to localization in lipid rafts. Many proteins are regulated by palmitoylation and PIP_2, including numerous inflammatory proteins.

Based on the significant inhibition of SARS2-PV entry from tetracaine and propofol, a local anesthetic and a general anesthetic, anesthetic-like chemicals have great potential to treat COVID-19. The similarities between HCQ and anesthetics in chemical structure, viral entry inhibition, and raft perturbation tempt us to hypothesize that both HCQ and anesthetics share a parallel mechanism of action. Also, CQ has side effects similar to those reported in anesthetics[44]. Therefore, anesthetists and the vast knowledge of anesthesiology may be useful when administrating HCQ to patients, especially in high doses.

All the imaging was performed with endogenously expressed proteins since overexpression can greatly affect movement of the proteins in and out of GM1 lipid rafts. The lipids were labeled after fixing to reduce movement between domains during labeling and to limit potential local lipid clustering by CTxB, especially saturated lipids. CTxB is pentadentate and in unfixed lipids causes clustering[45] and to some degree CTxB clustering occurs in fixed cells[46]. Since we examined disruption of lipids, the CTxB could have decreased the amount of disruption we reported for apparent GM1 raft size (i.e., the amount of disruption may be under reported). PIP_2 is polyunsaturated and we expect it is much better fixed in the membrane.

METHODS

Reagents

Hydroxychloroquine was purchase from Cayman Chemical and tetracaine was purchased from Sigma-Aldrich. Purified PLD2 from cabbage was purchased from Sigma-Aldrich respectively. PLD assay reagent amplex red 10-Acetyl-3,7-dihydroxyphenoxazine and 2-dioctanoyl-sn-glycero-3-phosphocholine (C8-PC) were purchased from Cayman Chemical. Horseradish peroxidase and choline oxidase were purchased from VWR. Methylbetacyclodextrin (MβCD) was purchased from Sigma-Aldrich.

Psuedo-typed SARS-CoV-2 (SARS2-PV) Viral Entry Assay

Cells and virus

HEK293T cell line was cultured in Dulbecco's Modified Eagle Medium (DMEM) with 10% fetal bovine serum (FBS) at 37 °C with 5% CO_2 atmosphere. SARS-CoV-2 pseudotyped particles were constructed using plasmid co-transfection, and the particles were maintained at -80°C. The constructs were a gift from Dr. Mike Farzan, Scripps Research, Florida. Evaluation of antiviral activities HEK293T ACE2 overexpression cells (0.5 × 105 cells/well), also provided by Dr. Mike Farzan, were cultured in 96-well cell-culture plates (Corning™ Coastar™ Cell Culture 96 well plates, #3585) were incubated with 100 µL pseudotyped particles of each type, together with 50 µM hydroxychloroquine sulfate (HCQ, Cayman, #17911) or 50 µM tetracaine hydrochloride (Sigma-Aldrich, #T7508) for 1 h. Then, the virus-drug mixture was removed, and fresh medium was added. After 24 h, the particles yields were determined through a luciferase assay. Cells were washed with PBS and 16 µL Cell Culture Lysis Reagent (Promega, #E153A) was added into each well. The plate was incubated for 15 min with rocking at room temperature. 8 µL of cell lysate from each well was added into a 384-well plate, followed by the addition of 16 µL of Luciferase Assay Substrate (Promega, #E151A). Luciferase activity measurement was performed on a Spark 20M multimode microplate reader (Tecan). The luciferase activity as infection yields were plotted in GraphPad Prism 6 software. All the infection experiments were performed in a biosafety level-2 (BLS-2) laboratory.

Super Resolution Microscopy (dSTORM)

To detect the lipid raft perturbation by hydroxychloroquine we employed Super Resolution Microscopy as described previously[11]. Briefly, HEK293T cells were grown in 8-well chamber slides (Nunc Lab-Tek chamber slide system, Thermo Scientific), washed and treated with 30-50 µM hydroxychloroquine for 30 min. The cells were then fixed with 3% paraformaldehyde, 0.1% glutaraldehyde, 30-50 µM hydroxychloroquine for 20 min, quenched with 0.1% $NaBH_4$ for 7 min. Cells were then washed with PBS (three times) and permeabilized with 0.2% Triton-X 100 in PBS for 15 min. The permeabilized cells were blocked using a standard blocking buffer containing 10% BSA and 0.05% Triton in PBS for 90 min. For labelling, cells were incubated with primary antibody (anti-ACE2 antibody (Abcam, #ab189168), anti-PLD2 antibody, or anti- PIP_2 antibody) for 60 min in antibody buffer (PBS with 5% BSA and 0.05% TritonX-100) at room temperature followed by 5 washes with wash buffer (PBS with 1% BSA and 0.05% TritonX-100) for 15 min each. Secondary antibodies (donkey anti-rabbit Cy3B and Alexa 647 conjugated CTxB) were added with antibody buffer for 30 min at room temperature followed by 5 washes as stated above. Then, cells were washed with PBS for 5 min and fixed for 10 min with fixation buffer as above, followed by 5 min washes with PBS for 3 times and 3 min washes with deionized distilled water. All steps except for pre- and post-fixation were performed with shaking.

A Zeiss Elyra PS1 microscope was used for super resolution microscopy with an oil-immersed 63X objective lens in TIRF mode. Images were acquired by Andor iXon 897 EMCCD camera and Zen 10D software with an exposure time of 18 ms per acquisition. Total 7,000-10,000 frames were collected. Alexa Fluor 647 and Cy3B were excited with a 642 nm and 561 nm laser in a photo-switching buffer consisting 1% betamercaptoethanol, 0.4 mg glucose oxidase and 23.8 µg catalase (oxygen scavengers), 50 mM Tris, 10 mM NaCl, and 10% glucose at pH 8.0. Localization drifts were corrected with n autocorrelative algorithm[47]. The drift-corrected coordinates were converted to be compatible to Vutara SRX software by an Excel macro. Cluster analysis and cross pair correlations were determined with the default modules in Vutara SRX software. DBSCAN algorithm was applied to determine the clusters which are within the search radius (ε) of 100 nm and consisting of at least 10 localizations. The apparent raft size was calculated by measuring the full width half max (FWHM) of the clusters.

Sandwich ELISA assay

HEK293T cells were cultured in 96-well cell-culture plates. Each well was incubated with and without 100 mL treatments for 1 h, then washed with 100 mL PBS once and incubated with 100 mL PBS for 1 h. Supernatants were collected and analyzed for Aβ40 ELISA.

A 96-well plate was coated with 50 mL capture antibody (IBL #11088) at 5 mg/ml concentration in PBS and incubated overnight at 4°C. All of the rest incubations were performed at room temperature. The plate was washed with 200 mL PBS for three times, and 100 mL blocking buffer (PBS with

10%BSA and 0.05% TritonX-100) was added to each well and incubated for 1 h. Next, the blocking buffer was removed, and 50 mL of supernatant was added to each well and incubated for 1 h, followed by an addition of 50 mL primary antibody (Invitrogen™ #PA3-16760) at 1:10000 dilution in PBST buffer (PBS with 0.01% TritonX-100). After a 3 h incubation, the plate was washed with 200 mL PBST for 4 times and 100 mL HRP-linked goat anti-rabbit IgG secondary antibody (Invitrogen™ #31460) at 0.4 mg/ml concentration in PBST buffer was added for 1 h incubation in the dark. Then, the plate was washed with 200 mL PBST for 4 times. 80 mL Chromogen (Invitrogen™ #002023) was added and incubated in the dark for 30 min. Finally, 80 mL stop solution (Invitrogen™ #SS04) was applied to terminate the substrate development. Measurement of absorbance at 450 nm was performed on a microplate reader (Tecan Infinite 200 PRO) to determine relative Ab40 concentration.

Membrane Fluidity Test

Change of membrane fluidity of HEK 293T cells was measured using the Membrane Fluidity kit (Abcam) following the manufacturer's protocol. Briefly, ~10,000 cells were seed in 96 well plates and incubated with the drugs and the fluorescent lipid reagent containing pyrenedecanoic acid (2 mM) at the room temperature for 20-30 mins. with. Pyrenedecanoic acid exists as either a monomer or an excimer, the latter forms due to the change in the membrane fluidity. The formation of the excimers shifts the emission spectrum of the pyrene probe to the longer wavelength. The changes in spectrum emission were measured with a fluorescence microplate reader (Tecan Infinite 200 Pro). The ratio of monomer (EM 372 nm) to excimer (EM 470 nm) fluorescence was calculated to obtain a quantitative change of the membrane fluidity.

In vivo and *in vitro* PLD Assay

In vivo PLD2 activity was measured in cultured HEK 293T cells by an enzyme-coupled product release assay using amplex red reagent as described previously[11]. Cells were seeded into 96-well plates (~5×10^4 cells per well) and incubated at 37 °C overnight to reach confluency. The cells were starved with serum-free DMEM for a day and washed once with PBS (phosphate-buffered saline). The PLD reaction was initiated by adding 100 µL of reaction buffer (100 µM amplex red, 2 U/ml horseradish peroxidase (HRP), 0.2 U/ml choline oxidase, and 60 µM C8-PC, 50 mM HEPES, and 5 mM CaCl2, pH 8.0). The assay reaction was performed for 2-4 hour at 37 °C and the activity was kinetically measured with a fluorescence microplate reader (Tecan Infinite 200 Pro) at excitation and emission wavelengths of 530 nm and 585 nm, respectively. For *in vitro* assay, cabbage PLD was used instead of the live cells and the PLD reaction was initiated as described for the *in vivo* assay. The PLD2 activity was calculated by subtracting the background activity (reaction buffer with the drugs, but no cells). For the bar graphs, samples were normalized to the control activity at the 120 min time point.

Statistical Analyses

Data calculations and graphs were performed in Prism 6 (GraphPad software) or Microsoft Excel. Experiments were done two-three times to ensure reproducibility. All Experimental samples were performed in random orders when to avoid any experimental bias. To ensure the reproducible effect of the sample sizes, super resolution imaging was carried out on multiple cells. Statistical significance was evaluated using ANOVA with post hoc Dunnett's test, two-tailed t-tests, parametric or nonparametric wherever appropriate. Data are shown as the mean and the error bars with SD. Significance is indicated by *P ≤ 0.05, **P ≤ 0.01, ***P ≤ 0.001, and ****P ≤ 0.0001.

Conflicts of Interests/Financial Disclosures: NONE

CONTRIBUTIONS

ZY and HW performed viral entry assays, ZY and MAP performed imaging experiments, and ZY performed the Aβ experiments with the help of HW. ZY, MAP, and SBH designed the experiments and wrote the manuscript.

Funding Statement: This work was supported by the National Institutes of Health with an R01 to S.B.H. (R01NS112534) and the US Department of Defense with an Accelerating Innovation in Military Medicine to S.B.H. (W81XWH1810782). We are grateful Mike Farzan for providing SARS2-PV and to the Iris and Junming Le Foundation for funds to purchase a super-resolution microscope, making this study possible.

References

1. Sohrabi C, Alsafi Z, O'Neill N, Khan M, Kerwan A, Al-Jabir A, Iosifidis C, Agha R. World Health Organization declares global emergency: A review of the 2019 novel coronavirus (COVID-19). Int J Surg 2020;76:71–6.
2. Liu J, Cao R, Xu M, Wang X, Zhang H, Hu H, Li Y, Hu Z, Zhong W, Wang M. Hydroxychloroquine, a less toxic derivative of chloroquine, is effective in inhibiting SARS-CoV-2 infection in vitro. Cell Discov 2020;6:1–4.
3. Chen Z, Hu J, Zhang Z, Jiang S, Han S, Yan D, Zhuang R, Hu B, Zhang Z. Efficacy of hydroxychloroquine in patients with COVID-19: results of a randomized clinical trial. medRxiv 2020:2020.03.22.20040758.
4. Wang M, Cao R, Zhang L, Yang X, Liu J, Xu M, Shi Z, Hu Z, Zhong W, Xiao G. Remdesivir and chloroquine effectively inhibit the recently emerged novel coronavirus (2019-nCoV) in vitro. Cell Res 2020;30:269–71.
5. Cortegiani A, Ingoglia G, Ippolito M, Giarratano A, Einav S. A systematic review on the efficacy and safety of chloroquine for the treatment of COVID-19. J Crit Care 2020.
6. Gautret P, Lagier J, Parola P, Hoang VT, Meddeb L, Mailhe M, Doudier B, Courjon J, Giordanengo V, Vieira VE, Dupont HT, Honoré S, Colson P, Chabrière E, Scola B La, Rolain J, Brouqui P, Raoult D. Hydroxychloroquine and azithromycin as a treatment of COVID-19: results of an open-label non-randomized clinical trial. Int J Antimicrob Agents 2020:105949. Available at: https://linkinghub.elsevier.com/retrieve/pii/S0924857920300996.
7. Ledford H. Safety fears over drug hyped to treat the coronavirus spark global confusion. Nature 2020;582:18–9. Available at: http://www.nature.com/articles/d41586-020-01599-9.
8. Sullivan DJ, Gluzman IY, Russell DG, Goldberg DE. On the molecular mechanism of chloroquine's antimalarial action. Proc Natl Acad Sci U S A 1996;93:11865–70.
9. Senthilkumaran S, Koushik M, Sanjay P, Thirumalaikolundusubramanian P. Propofol in COVID 19 — From basic science to clinical impact. Am J Emerg Med 2020. Available at: https://linkinghub.elsevier.com/retrieve/pii/S0735675720306033.
10. Pavel MA, Petersen EN, Wang H, Lerner RA, Hansen SB. Studies on the mechanism of general anesthesia. Proc Natl Acad Sci U S A 2020;117:13757–66. Available at: http://www.ncbi.nlm.nih.gov/pubmed/32467161.
11. Petersen EN, Chung H-W, Nayebosadri A, Hansen SB. Kinetic disruption of lipid rafts is a mechanosensor for phospholipase D. Nat Commun 2016;7:13873. Available at: http://www.ncbi.nlm.nih.gov/pubmed/27976674.
12. Lingwood D, Simons K. Lipid rafts as a membrane-organizing principle. Science 2010;327:46–50. Available at: http://www.ncbi.nlm.nih.gov/pubmed/20044567. Accessed October 31, 2013.
13. Bogaart G van den, Meyenberg K, Risselada HJ, Amin H, Willig KI, Hubrich BE, Dier M, Hell SW, Grubmüller H, Diederichsen U, Jahn R. Membrane protein sequestering by ionic protein-lipid interactions. Nature 2011;479:552–5. Available at: http://www.nature.com/doifinder/10.1038/nature10545. Accessed October 6, 2014.
14. Pavel MAMA, Chung HH-W, Petersen ENN, Hansen SBSB. Polymodal Mechanism for TWIK-Related K+ Channel Inhibition by Local Anesthetic. Anesth Analg 2019;129:973–82. Available at: http://www.ncbi.nlm.nih.gov/pubmed/31124840.
15. Schmidt NM, Wing PAC, McKeating JA, Maini MK. Cholesterol-modifying drugs in COVID-19. Oxford Open Immunol 2020;1:1–6.
16. Li W, Moore MJ, Vasilieva N, Sui J, Wong SK, Berne MA, Somasundaran M, Sullivan JL, Luzuriaga K, Greenough TC, Choe H, Farzan M. Angiotensin-converting enzyme 2 is a functional receptor for the SARS coronavirus. Nature 2003;426:450–4. Available at: http://www.ncbi.nlm.nih.gov/pubmed/14647384.
17. Hoffmann M, Kleine-Weber H, Schroeder S, Krüger N, Herrler T, Erichsen S, Schiergens TS, Herrler G, Wu N-HH, Nitsche A, Müller MA, Drosten C, Pöhlmann S. SARS-CoV-2 Cell Entry Depends on ACE2 and TMPRSS2 and Is Blocked by a Clinically Proven Protease Inhibitor. Cell 2020;181:271-280.e8. Available at: https://doi.org/10.1016/j.cell.2020.02.052. Accessed April 1, 2020.
18. Wang H, Yuan Z, Pavel MA, Hansen S. The role of high cholesterol in aged related COVID19 lethality. bioRxiv 2020:2020.05.09.086249. Available at:

http://biorxiv.org/content/early/2020/05/10/2020.05.09.086249.1.abstract.
19. Lespinasse BVD. Quinine and Urea hydrochlorate as a local anesthetic. Med Sch Bull Northwest Univ 1910:161–3.
20. Dronsfield A, Ellis P. Quinine-Urea, a Short-lived, Long-acting Local Anaesthetic? J Anesth Hist 2017;3:147.
21. Krogstad DJ, Schlesinger PH. The basis of antimalarial action: Non-weak base effects of chloroquine on acid vesicle pH. Am J Trop Med Hyg 1987;36:213–20.
22. Kumar M, Chawla R, Goyal M. Topical anesthesia. J Anaesthesiol Clin Pharmacol 2015;31:450–6.
23. Cervin M, Anderson R. Modulation of coronavirus-mediated cell fusion by homeostatic control of cholesterol and fatty acid metabolism. J Med Virol 1991;35:142–9.
24. Guo H, Huang M, Yuan Q, Wei Y, Gao Y, Mao L, Gu L, Tan YW, Zhong Y, Liu D, Sun S. The important role of lipid raft-mediated attachment in the infection of cultured cells by coronavirus infectious bronchitis virus beaudette strain. PLoS One 2017;12:1–12.
25. Miller DK, Lenard J. Antihistaminics, local anesthetics, and other amines as antiviral agents. Proc Natl Acad Sci U S A 1981;78:3605–9.
26. Hollmann MW, Durieux ME, Fisher DM. Local anesthetics and the inflammatory response: A new therapeutic indication? Anesthesiology 2000;93:858–75.
27. Quinlan BD, Mou H, Zhang L, Guo Y, He W, Ojha A, Parcells MS, Luo G, Li W, Zhong G, Choe H, Farzan M. The SARS-CoV-2 receptor-binding domain elicits a potent neutralizing resonse without antibody-dependent enhancement. bioRxiv 2020:1–9.
28. Moore MJ, Dorfman T, Li W, Wong SK, Li Y, Kuhn JH, Coderre J, Vasilieva N, Han Z, Greenough TC, Farzan M, Choe H. Retroviruses Pseudotyped with the Severe Acute Respiratory Syndrome Coronavirus Spike Protein Efficiently Infect Cells Expressing Angiotensin-Converting Enzyme 2. J Virol 2004;78:10628–35.
29. Kuo C-L, Pilling LC, Atkins JL, Masoli JAH, Delgado J, Kuchel GA, Melzer D. APOE e4 genotype predicts severe COVID-19 in the UK Biobank community cohort. Journals Gerontol Ser A 2020:1–29. Available at: https://academic.oup.com/biomedgerontology/advance-article/doi/10.1093/gerona/glaa131/5843454.
30. Luo J, Yang H, Song BL. Mechanisms and regulation of cholesterol homeostasis. Nat Rev Mol Cell Biol 2020;21:225–45.
31. Petersen EN, Clowes KR, Hansen SB. Measuring anesthetic resistance in Drosophila by VAAPR. bioRxiv 2019.
32. Hansen SB. Lipid agonism: The PIP2 paradigm of ligand-gated ion channels. Biochim Biophys Acta 2015;1851:620–8. Available at: http://www.ncbi.nlm.nih.gov/pubmed/25633344. Accessed February 6, 2015.
33. Robinson C V., Rohacs T, Hansen SB. Tools for Understanding Nanoscale Lipid Regulation of Ion Channels. Trends Biochem Sci 2019;44:795–806. Available at: https://linkinghub.elsevier.com/retrieve/pii/S0968000419300817. Accessed May 3, 2019.
34. Arshad S, Kilgore P, Chaudhry ZS, Jacobsen G, Wang DD, Huitsing K, Brar I, Alangaden GJ, Ramesh MS, McKinnon JE, O'Neill W, Zervos M, Nauriyal V, Hamed AA, Nadeem O, Swiderek J, Godfrey A, Jennings J, Gardner-Gray J, Ackerman AM, Lezotte J, Ruhala J, Fadel R, Vahia A, Gudipati S, Parraga T, Shallal A, Maki G, Tariq Z, Suleyman G, et al. Treatment with hydroxychloroquine, azithromycin, and combination in patients hospitalized with COVID-19. Int J Infect Dis 2020;97:396–403.
35. Gosztyla ML, Brothers HM, Robinson SR. Alzheimer's Amyloid-β is an Antimicrobial Peptide: A Review of the Evidence. J Alzheimer's Dis 2018;62:1495–506.
36. Kumar DKV, Choi SH, Washicosky KJ, Eimer WA, Tucker S, Ghofrani J, Lefkowitz A, McColl G, Goldstein LE, Tanzi RE, Moir RD. Amyloid-β peptide protects against microbial infection in mouse and worm models of Alzheimer's disease. Sci Transl Med 2016;8:340ra72. Available at: http://www.ncbi.nlm.nih.gov/pubmed/27225182. Accessed March 22, 2019.
37. Tall AR, Yvan-Charvet L. Cholesterol, inflammation and innate immunity. Nat Rev Immunol 2015;15:104–16. Available at: http://www.nature.com/articles/nri3793.
38. Wang H, Kulas JA, Ferris HA, Hansen SB. Regulation of amyloid processing in neurons by astrocyte-derived cholesterol. bioRxiv 2020:2020.06.18.159632. Available at: http://biorxiv.org/content/early/2020/06/18/2020.06.18.159632.abstract.

39. Ehehalt R, Keller P, Haass C, Thiele C, Simons K. Amyloidogenic processing of the Alzheimer β-amyloid precursor protein depends on lipid rafts. J Cell Biol 2003;160:113–23.
40. Sieben C, Sezgin E, Eggeling C, Manley S. Influenza A viruses use multivalent sialic acid clusters for cell binding and receptor activation. PLoS Pathog 2020;16:e1008656.
41. Hansen SB, Tao X, MacKinnon R. Structural basis of PIP2 activation of the classical inward rectifier K+ channel Kir2.2. Nature 2011;477:495–8. Available at: http://www.ncbi.nlm.nih.gov/pubmed/21874019. Accessed August 29, 2011.
42. Fantini J, Scala C Di, Chahinian H, Yahi N. Structural and molecular modeling studies reveal a new mechanism of action of chloroquine and hydroxychloroquine against SARS-CoV-2 infection. Int J Antimicrob Agents 2020:105960.
43. Li GM, Li YG, Yamate M, Li SM, Ikuta K. Lipid rafts play an important role in the early stage of severe acute respiratory syndrome-coronavirus life cycle. Microbes Infect 2007;9:96–102. Available at: http://www.ncbi.nlm.nih.gov/pubmed/17194611. Accessed March 29, 2020.
44. Borba MGS, Val FFA, Sampaio VS, Alexandre MAA, Melo GC, Brito M, Mourão MPG, Brito-Sousa JD, Baía-da-Silva D, Guerra MVF, Hajjar LA, Pinto RC, Balieiro AAS, Pacheco AGF, Santos JDO, Naveca FG, Xavier MS, Siqueira AM, Schwarzbold A, Croda J, Nogueira ML, Romero GAS, Bassat Q, Fontes CJ, Albuquerque BC, Daniel-Ribeiro CT, Monteiro WM, Lacerda MVG. Effect of High vs Low Doses of Chloroquine Diphosphate as Adjunctive Therapy for Patients Hospitalized With Severe Acute Respiratory Syndrome Coronavirus 2 (SARS-CoV-2) Infection: A Randomized Clinical Trial. JAMA Netw open 2020;3:e208857.
45. Moon S, Yan R, Kenny SJ, Shyu Y, Xiang L, Li W, Xu K. Spectrally Resolved, Functional Super-Resolution Microscopy Reveals Nanoscale Compositional Heterogeneity in Live-Cell Membranes. J Am Chem Soc 2017;139:10944–7. Available at: https://pubs.acs.org/doi/10.1021/jacs.7b03846. Accessed August 26, 2019.
46. Petersen EN, Pavel MA, Wang H, Hansen SB. Disruption of palmitate-mediated localization; a shared pathway of force and anesthetic activation of TREK-1 channels. Biochim Biophys Acta - Biomembr 2020;1862:183091. Available at: https://linkinghub.elsevier.com/retrieve/pii/S0005273619302378. Accessed November 8, 2019.
47. Mlodzianoski MJ, Schreiner JM, Callahan SP, Smolková K, Dlasková A, Santorová J, Ježek P, Bewersdorf J. Sample drift correction in 3D fluorescence photoactivation localization microscopy. Opt Express 2011;19:15009–19. Available at: http://www.ncbi.nlm.nih.gov/pubmed/21934862.
48. Honigmann A, Pralle A. Compartmentalization of the Cell Membrane. J Mol Biol 2016;428:4739–48.

Supplemental Figures

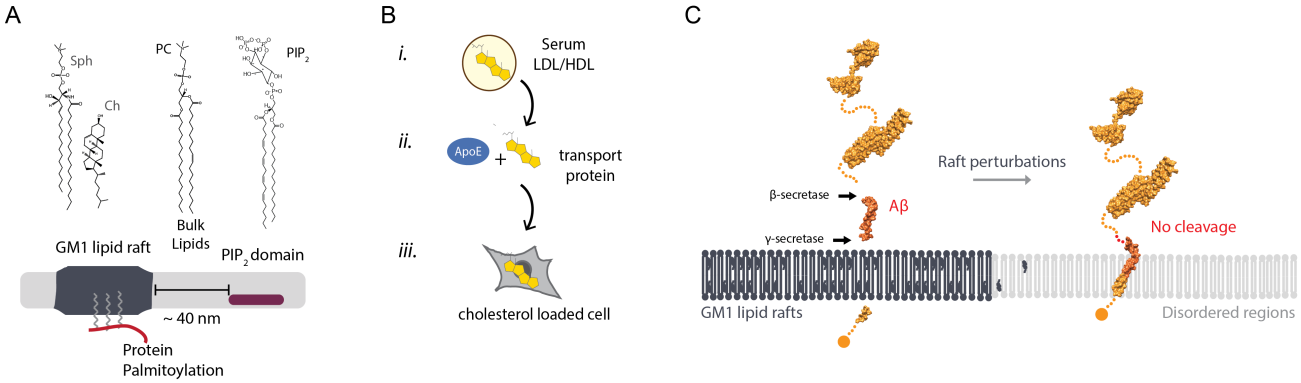

Fig. S1. Membrane heterogeneity. (A) GM1 rafts are clusters of saturated known as liquid ordered (L_o) and commonly reside separate from liquid disordered (L_d) phases[46]. The ordered phase (L_o) is generally enriched in sphingomyelin and cholesterol whereas the disordered (L_d) phase consists of unsaturated lipids and includes polyunsaturated lipids like PA and PIP_2[48]. **(B)** Cartoon diagram showing the experimental setup for loading cultured cells with cholesterol. ***i.***, Cholesterol (yellow shading) loaded into lipoprotein (e.g., low- and high-density lipoprotein (LDL and HDL respectively)) from blood serum. ***ii.***, Cholesterol free human apolipoprotein E (apoE, brown shading), a cholesterol transport protein, is exposed to cholesterol from blood serum and ***iii,*** ApoE transports cholesterol into of cells (grey shading). **(C)** Model of HCQ and anesthetics translocating APP from GM1 rafts to disordered regions through raft perturbation to reduce the synthesis of Ab.

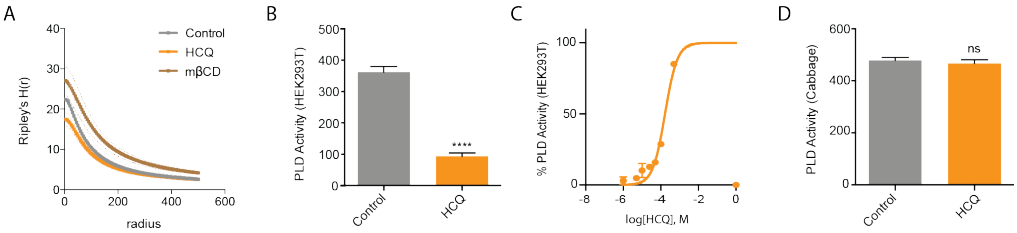

Fig. S2. HCQ displacement of PLD2 from lipid rafts. (A) Ripley's H -Function (H(r)) showing raft separation. **(B)** HCQ (50μM) decreased PLD activity in PLD assay. Data are expressed as mean ± s.e.m., ****P ≤ 0.0001, unpaired t test, n=6. **(C)** A dose response of HCQ's inhibition to PLD activity in PLD assay, n=3. **(D)** Effect of HCQ(50μM) on PLD activity in cabbage PLD assay is not significant, unpaired t test, n=4-5.

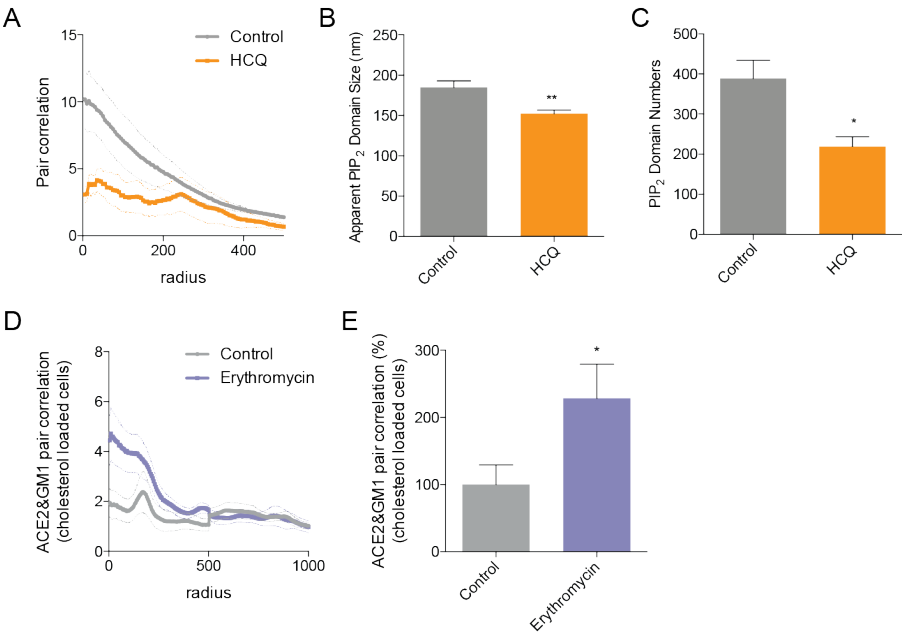

Fig. S3. dSTORM of PIP_2 domains. (**A**) Cross pair correlation analysis of dSTORM imaging (Fig. 3C). HCQ treatment decreased association of ACE2 and PIP_2. **(B-C)** Bar graph of the apparent raft diameter analyzed by DBSCAN cluster analysis. HCQ decreases both raft diameter (B) and number (C) of PIP_2 domains. Data are expressed as mean ± s.e.m., *P ≤ 0.05, **P ≤ 0.01, one-way ANOVA, n=5-6. **(D-E)** Cross pair correlation (D) and percent of cross pair correlation calculated at short distances (0-5 nm) (E) of dSTORM imaging. Erythromycin treatment decreased association of ACE2 with GM1 rafts. Data are expressed as mean ± s.e.m., *P ≤ 0.05, **P ≤ 0.01, unpaired t test, n=10.